Continuous wave, frequency-tunable terahertz laser radiation generated via stimulated polariton scattering

Andrew J. Lee* and Helen M. Pask

MQ Photonics Research Centre, Department of Physics and Astronomy, Macquarie University, NSW 2109, Australia
**Corresponding author: andrew.lee@mq.edu.au*

Received November 13, 2013; revised December 16, 2013; accepted December 17, 2013;
posted December 18, 2013 (Doc. ID 201310); published January 20, 2014

We report the generation of CW THz radiation, generated via stimulated polariton scattering in MgO:$LiNbO_3$. The system is capable of producing frequency tunable radiation across the range 1.5–2.3 THz and requires only 2.3 W incident diode pump power to reach threshold. Maximum THz output power of 2.3 μW has been detected for just 5.9 W incident diode pump power, at a frequency of 1.8 THz. © 2014 Optical Society of America

OCIS codes: (140.3550) Lasers, Raman; (140.3480) Lasers, diode-pumped; (140.3070) Infrared and far-infrared lasers; (190.2620) Harmonic generation and mixing; (190.4410) Nonlinear optics, parametric processes.
http://dx.doi.org/10.1364/OL.39.000442

With the ever-increasing number of applications for THz radiation, there is growing demand for THz sources that can generate high output power and different output modalities (pulsed and CW). For applications in imaging and spectroscopy, CW THz sources are often regarded as being better suited than pulsed sources because they can be more simply interfaced with detectors [1], and the linewidth of the emission can be made narrower (not being limited by the pulse duration transform limit), which may enable applications in high resolution spectroscopy [2,3]. CW THz sources have been demonstrated in the past, and such sources include those employing difference-frequency mixing of two lasers [4]; parametric generation [5]; and quantum cascade lasers [6].

One method that has proven effective at generating pulsed THz radiation with frequency-tunable output is terahertz parametric oscillation, most notably in MgO:$LiNbO_3$ [7–11]. The nonlinear interaction that generates the THz radiation involves both second- and third-order nonlinear processes [7–9], with the analysis in [9] showing the third-order interaction dominated (60%). For this reason, and as in our previous work [12] and that detailed in [13], we choose to describe this system as being based on stimulated polariton scattering (SPS). In these systems, a cavity is formed around an MgO:$LiNbO_3$ crystal to oscillate near-IR Stokes radiation, which is produced via SPS from the 248 cm^{-1} mode, when a high-intensity laser pulse, typically from a pulsed Nd:YAG laser, is incident on the crystal. The polaritons that are also generated in the process have frequencies in the 1–4 THz range that exit the MgO:$LiNbO_3$ crystal at an angle that satisfies conservation of momentum of the fundamental, Stokes, and polariton fields. These systems are capable of generating peak THz powers exceeding 1 kW [10]. Another, more efficient, means of producing THz radiation via SPS is to place the MgO:$LiNbO_3$ crystal within the cavity of a solid-state laser, to access the high intracavity fundamental field (typically at 1064 nm when a Nd^{3+}-doped crystal is used as the laser gain medium) [12,14]. In doing so, very modest diode pump powers are required to achieve SPS threshold, and we have reported a system that generates ns-pulsed THz emission for only 2.4 W incident diode pump power [12].

SPS systems are attractive as they can be based on robust Nd laser technology, operate at room temperature, are capable of broad frequency tuning, have relatively narrow linewidth, and in the case of intracavity configurations, have low pump power requirements. To date, however, these systems have only operated in the pulsed regime, with intracavity configurations using a Q-switch in order to achieve sufficiently high intensities for the nonlinear SPS process. In this Letter we report the first CW operation of an intracavity SPS system. To achieve this mode of operation, we utilize design cues from intracavity CW Raman lasers, demonstrate low threshold for THz generation, and generate output power up to 2.3 μW when pumping at up to 2.6 times above SPS threshold.

The THz SPS source reported here comprises a diode end-pumped Nd:$GdVO_4$ laser resonator with an intracavity MgO:$LiNbO_3$ crystal. A second resonator is formed around the MgO:$LiNbO_3$ crystal to resonate the Stokes radiation, and the system is designed so that this Stokes resonator can be rotated about the y axis of the MgO:$LiNbO_3$ crystal. Varying the angle between the two resonator axes enables frequency tuning of the Stokes and THz radiation. As with an end-pumped Raman laser, it is essential to achieve a high intracavity fundamental field intensity in the MgO:$LiNbO_3$ to reach threshold for the SPS process. Therefore, we make use of resonator mirrors with very high reflectivity at the fundamental and Stokes wavelengths, and we also make use of relatively small resonator modes (~500 μm diameter). An Nd:$GdVO_4$ laser crystal was used to generate a polarized fundamental field ($\lambda = 1063$ nm) within the laser cavity; it is aligned along the z axis of the MgO:$LiNbO_3$ to access the highest gain, 248 cm^{-1} polariton mode. The system layout is shown in Fig 1. The fundamental field resonator was pumped by an 808 nm, 30 W, fiber-coupled (200 μm core diameter, 0.22 NA) diode laser that was focused to a waist of 600 μm diameter onto the surface of the Nd:$GdVO_4$ crystal. The Nd:$GdVO_4$ crystal was cut for propagation along the a axis, had 0.3% a.t. Nd-doping,

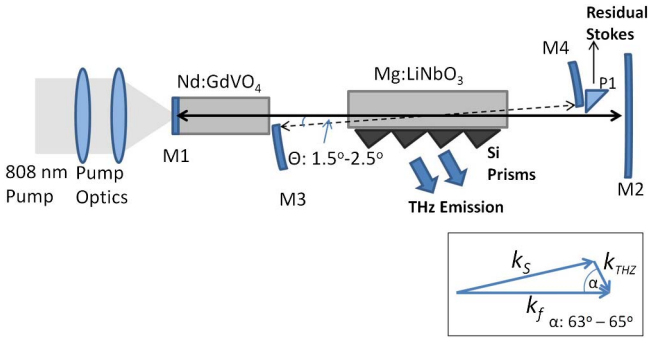

Fig. 1. System layout. Note that the distance between the interaction region of the fundamental, Stokes, and polariton (THz) fields, and the edge of the $MgO:LiNbO_3$ crystal is exaggerated for clarity, as is the angle between the fundamental (represented by the solid arrow) and Stokes (represented by the dashed arrow) fields. The wavevectors representing the interaction of the fundamental (k_f), Stokes (k_S), and THz (k_{THz}) fields involved in the SPS process is shown inset.

and had dimensions of 5 mm × 5 mm × 13 mm. An HR coating with $R \sim 99.994\%$ at 1063–1173 nm and $T > 99.930\%$ at 808 nm (as measured by the supplier) was applied directly to the input facet of the $Nd:GdVO_4$ crystal, forming the input mirror (M1) for the fundamental resonator. The fundamental resonator end mirror (M2) had a radius of curvature (ROC) of 500 mm and a HR coating with $R > 99.995\%$ at 1064 nm (based on transmission measurements we performed). The congruent $MgO:LiNbO_3$ crystal (sourced from HC Photonics Corp.) was x-cut, 5% a.t. MgO-doped, and had dimensions 5 mm × 5 mm × 25 mm. The 5% a.t. MgO-doping was used to ensure high damage threshold [15] and high SPS conversion efficiency [16].

The Stokes cavity was formed using two 1 m ROC D-shaped mirrors (to enable oscillation of the fundamental and Stokes fields without clipping), each HR coated $R \sim 99.999\%$ from 1060 to 1080 nm (as measured by the supplier). The total lengths of the fundamental and Stokes resonators were 185 and 115 mm, respectively. The Stokes resonator was mounted on a micrometer-driven rotation stage, to enable its rotation about the z axis of the $MgO:LiNbO_3$ crystal. In this way, SPS could be investigated for angles between around 1 and 3 deg, between the axes of the Stokes and fundamental field resonators. The minimum angle was limited by clipping of the fundamental field by the Stokes mirrors. The maximum angle was limited by the need to keep the interaction region of the fundamental, Stokes and THz fields close to the surface of the $MgO:LiNbO_3$ crystal interfaced with the Si prisms so as to minimize absorption of the THz field [16] before it exited the crystal. It was also limited by clipping of the Stokes field by the edge of the $MgO:LiNbO_3$ crystal. As depicted in Fig. 1, the THz radiation was generated at an angle of 63°–65° to the fundamental field resonator axis. Output-coupling of the generated THz field was facilitated by overcoming total internal reflection through the use of high-resistivity Si prisms ($R > 10\ k\Omega\,cm^{-1}$) adhered (using liquid-mediated adhesion [17]) to a polished surface of the $MgO:LiNbO_3$ crystal (perpendicular to the y axis of the crystal).

The fundamental resonator mode (TEM_{00}) diameter was estimated using ABCD resonator modeling [18], and varied from ~500 μm to 560 μm in the $MgO:LiNbO_3$ crystal, when the focal length of the thermal lens induced in the laser crystal was estimated to vary from 500 to 175 mm (these estimates are based on interferometric measurements on a similar end-pumped $Nd:GdVO_4$ laser crystal [19]). The modeling predicted that the fundamental field resonator would be stable for thermal lenses of focal length >170 mm. In the case of the Stokes cavity, the Stokes mode diameter was estimated to be ~540 μm.

The power scaling characteristics of the fundamental and Stokes fields were determined by directly measuring the near-IR radiation leaking through the output mirrors for each resonator (M2 and M4 for the fundamental and Stokes respectively). Observation of the Stokes field was enabled through the use of a small right angle prism (P1). Depletion of the fundamental field was determined through measurement of the fundamental field (leaking through M2) when the Stokes resonator was aligned to produce maximum detectable THz signal, and then completely misaligned (no Stokes/THz generation), the relative difference representing the depleted portion of the fundamental field. The power of the out-coupled THz field was measured using a calibrated Golay cell (Tydex Inc), and a mechanical chopper set at a frequency of 20 Hz with 50% duty-cycle. A layer of Teflon and black polyethylene were used to prevent residual near-IR radiation being detected by the Golay cell. The frequency of the generated THz radiation was inferred from the difference between the wavelengths of the fundamental (1063 nm) and Stokes fields, which varied with angle (θ) between the Stokes and fundamental field resonators.

Threshold for fundamental (1063 nm) field oscillation was reached for an incident diode pump power of 0.90 W, and threshold for oscillation of the Stokes (1070.0 nm) was reached for an incident diode pump power of 2.30 W. For this cavity configuration, there is a compromise between the maximum output power that can be detected (due to strong absorption within the $MgO:LiNbO_3$ crystal) and the achievable frequency-tuning range, which is limited for reasons already discussed. To determine the intracavity intensity of the fundamental field in the $MgO:LiNbO_3$, we first measured the transmission of mirror M2, by placing it in the path of a 2 W, $Nd:GdVO_4$ 1063 nm laser. A transmitted power of 35 μW ± 15 μW was measured, yielding a transmission value of 0.00175% ± 0.00075%. From this value, along with measurement of the residual fundamental power leaking through mirror M1, and the fundamental mode diameter of 500 μm in the $MgO:LiNbO_3$ crystal, it was determined that an intracavity fundamental field intensity of $0.22 \pm 0.16\ MW/cm^2$ was required in order to reach SPS threshold in this system. This intracavity intensity is an order of magnitude lower than that required to reach threshold in the pulsed system we reported previously [12]. This difference is attributed to the lower losses within the CW Stokes cavity used in this work, as the power required to reach Stokes threshold is directly proportional to the resonator loss [20].

The power-scaling properties of the laser are shown in Fig. 2, where the power of the residual fundamental and Stokes fields through mirrors M2 and M4, respectively, are plotted, along with the detected THz power as a function of incident diode pump power. In this case,

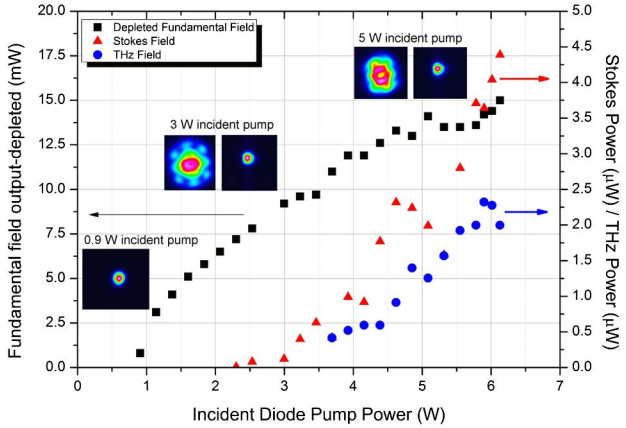

Fig. 2. Power scaling properties of the depleted fundamental, Stokes and THz fields, with the Stokes resonator angled to generate 1.83 THz emission. Shown inset are mode profiles of the fundamental (left) and Stokes (right) fields at incident pump powers of 0.9 W, 3 W and 5 W; note that the Stokes field is not present for an incident pump power of 0.9 W (below SPS threshold).

the angle between the Stokes and fundamental field resonators was fixed so as to generate THz emission at 1.83 THz. The alignment of the fundamental and Stokes resonators was, however, optimized for maximum THz generation/detected THz signal with each change in incident diode pump power. The lowest detectable THz signal using the Golay cell is ~0.3 μW (noise limit); hence the THz power scaling curve in Fig. 2 does not reach 0 μW.

Figure 2 shows how the Stokes and THz fields increase rapidly in power once above SPS threshold. The THz field increased to a maximum of 2.3 μW, for which the incident pump power was 5.9 W (~2.6 times the SPS threshold). A rapid decline in output power is observed thereafter, this being accompanied by significant instability of the fundamental field. This behavior is a consequence of the strong thermal lensing in the Nd:$GdVO_4$, which causes the resonator to approach its stability limit. We also observed that the fundamental field power does not clamp for incident pump powers above the SPS threshold (2.3 W). Rather, it continues to increase. This is a sign that the SPS process is not operating as efficiently as we would like. Using a laser beam profiler (Thorlabs BC106-VIS), we observed that above threshold for SPS, the fundamental field includes high-order modes (see inset of Fig. 2), and that as the incident pump power increases, the mode structure becomes increasingly distorted. Interestingly, there was no observed change in the mode profile of the Stokes field as the incident pump power increased, and it appeared to always oscillate as a TEM_{00} mode. It is interesting to note that clamping was observed in our earlier work [12] on a pulsed laser with intracavity SPS and also that such beam distortion of the fundamental field did not occur.

By intentionally aligning and misaligning mirror M3, we were able to switch the SPS process on and off and observe the change to the fundamental field leaking through mirror M2. By this means, a maximum fundamental field depletion of ~36% was measured. As the incident (diode) pump power increased, so did the depletion rate of the fundamental field, up until around a pump power of 5 W. We note this depletion is much lower than the 57% depletion observed using the same method for the aforementioned pulsed laser [12]. We believe that the lower efficiency observed in this system is due to the fundamental field instead operating on high-order transverse modes (as already discussed), which yields poor overlap between the fundamental and Stokes modes and hence results in lower conversion efficiency and no clamping of the fundamental field (only a reduction in the gradient of the power-scaling curve) once above SPS threshold.

The cause of the distortion of the fundamental field is presently unclear. It may include contributions from nonlinear self-defocusing and free-carrier-induced photorefractive effects within the MgO:$LiNbO_3$ crystal [21]. It is well documented that nonlinear self-defocusing manifests in congruent MgO:$LiNbO_3$ crystals (as used in this work), at relatively modest powers, and these effects can lead to significant distortion of the propagating beam [21,22]. Also, the fact that high-order mode oscillation and distortions manifest strongly in the CW regime, and were not observed at all in our pulsed system [12], suggests that photorefractive effects may also be involved. The pulsed system operated with a repetition rate of 3 kHz and pulse duration of ~10 ns. While the MgO dopant in MgO:$LiNbO_3$ is intended to avoid photorefractive damage (PRD) due to the bulk photorefractive effect, Schwesyg *et al.* [23], showed that pyroelectrically induced PRD did occur in MgO:$LiNbO_3$. By the inelastic nature of the SPS process, there is inevitably some heating of the MgO:$LiNbO_3$, and hence our CW laser is conducive to pyroelectrically induced PRD, which is shown in [23] to result in strong defocussing with effective focal length around a few cm.

We have insufficient evidence at this stage to definitively identify the origin of the beam distortions we observe. However, either self-defocusing or PRD could bring about these beam profiles.

We examined the spectrum of the residual fundamental and Stokes fields using a high resolution fiber-coupled spectrometer (Ocean Optics HR4000). We found that as the pump power was increased, the only spectral lines present were those of the fundamental and Stokes fields; no spurious lines, such as those originating from shifting along other Stokes lines, were present. The FWHM linewidth of the fundamental and Stokes fields were measured to be ~0.47 nm (125 GHz) and ~0.28 nm (72 GHz), respectively, and they did not change with incident pump power. The relatively broad linewidth of the fundamental field is attributed to the large number of longitudinal modes supported within the high-Q resonator. From these measurements, we inferred that the linewidth of the THz radiation was <72 GHz [24].

The frequency-tuning characteristics of this laser were investigated for an incident diode pump power of 5.2 W (this power was chosen to yield high THz output power, and yet remain below the resonator stability limit). The tuning curve is shown in Fig. 3, and shows that THz emission was obtained over a range 1.5—2.3 THz. The THz power increases rapidly from 1.5 THz, reaching a maximum at ~1.8 THz and then decreases as the frequency increases toward 2.4 THz. The rapid increase

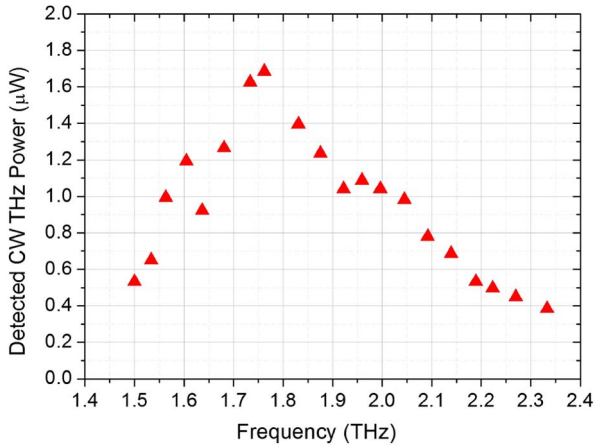

Fig. 3. Change in detected THz power as a function of THz field frequency. Input pump power was set to 5.2 W.

in output power at frequencies between 1.5 and 1.8 THz is consistent with increase in the SPS gain [16], while the decrease in THz output is due to increased THz absorption within the MgO:$LiNbO_3$ crystal at higher frequencies [16] and decreased overlap between the fundamental and Stokes fields. As mentioned earlier, the geometry of the laser leads to a trade-off between the maximum THz power and tunability.

In summary, we have demonstrated for the first time CW operation of an intracavity SPS laser generating frequency-tunable THz output. The system operates with very low threshold (2.3 W) and generates up to 2.3 μW emission at 1.8 THz, with frequency tunable THz output across the range 1.5—2.3 THz. Strong thermal lensing in the Nd:$GdVO_4$ laser crystal could be managed using in-band pumping at 879 nm [19,25], enabling power scaling. However, the most crucial factor is to understand the origin of the beam distortion that we have observed, and to devise strategies for managing it.

References

1. A. W. Lee and Q. Hu, Opt. Lett. **30**, 2563 (2005).
2. N. Karpowicz, H. Zhong, J. Xu, K.-I. Lin, J.-S. Hwang, and X.-C. Zhang, Semicond. Sci. Tech. **20**, S293 (2005).
3. T. M. Korter and D. F. Plusquellic, Chem. Phys. Lett. **385**, 45 (2004).
4. M. Scheller, J. M. Yarborough, J. V. Moloney, M. Fallahi, M. Koch, and S. W. Koch, Opt. Express **18**, 27112 (2010).
5. R. Sowade, I. Breunig, I. C. Mayorga, J. Kiessling, C. Tulea, V. Dierolf, and K. Buse, Opt. Express **17**, 22303 (2009).
6. B. S. Williams, S. Kumar, and Q. Hu, Opt. Express **13**, 3331 (2005).
7. J. Gelbwachs, R. H. Pantell, H. E. Puthoff, and J. M. Yaborough, Appl. Phys. Lett. **14**, 258 (1969).
8. M. A. Piestrup, R. N. Fleming, and R. H. Pantell, Appl. Phys. Lett. **26**, 418 (1975).
9. K. Kawase, J. Shikata, and H. Ito, J. Phys. D **34**, R1 (2001).
10. S. Hayashi, K. Nawata, K. Kawase, and H. Minamide, *Proceedings of the 37th International Conference on Infrared, Millimeter, and Terahertz Waves (IRMMW-THZ)*, Australia, September 22–28, 2012.
11. D. L. Mills and E. Burstein, Rep. Progr. Phys. **37**, 817 (1974).
12. A. J. Lee, Y. He, and H. M. Pask, IEEE J. Quantum Electron. **49**, 357 (2013).
13. C.-P. Xia, X.-F. Li, H.-J. Liu, and N. Huang, Laser Phys. **19**, 1897 (2009).
14. T. J. Edwards, D. Walsh, M. B. Spurr, C. F. McRae, M. H. Dunn, and P. G. Browne, Opt. Express **14**, 1582 (2006).
15. M. Nakamura, S. Higuchi, S. Takekawa, K. Terabe, Y. Furukawa, and K. Kitamura, Jpn. J. Appl. Phys. **41**, L49 (2002).
16. J.-I. Shikata, K. Kawase, K.-I. Karino, T. Taniuchi, and H. Ito, IEEE Trans. Microwave Theory Tech. **48**, 653 (2000).
17. E. Yablonovitch, D. M. Hwang, T. J. Gmitter, L. T. Florez, and J. P. Harbison, Appl. Phys. Lett. **56**, 2419 (1990).
18. Lascad-Software for Laser Cavity Analysis and Design. [Online]. Available: www.lac-cad.com
19. T. Omatsu, M. Okida, A. J. Lee, and H. M. Pask, Appl. Phys. B **108**, 73 (2012).
20. D. J. Spence, P. Dekker, and H. M. Pask, IEEE J. Quantum Electron. **13**, 756 (2007).
21. Q. Wang Song, C. Zhang, and P. J. Talbot, Appl. Opt. **32**, 7266 (1993).
22. L. Palfalvi, G. Almasi, J. Hebling, A. Peter, and K. Polgar, Appl. Phys. Lett. **80**, 2245 (2002).
23. J. R. Schwesyg, M. Falk, C. R. Phillips, D. H. Jundt, K. Buse, and M. M. Fejer, J. Opt. Soc. Am. B **28**, 1973 (2011).
24. D. J. M. Stothard, T. J. Edwards, D. Walsh, C. L. Thomson, C. F. Rae, M. H. Dunn, and P. G. Browne, Appl. Phys. Lett. **92**, 141105 (2008).
25. Y. Sato, T. Taira, N. Pavel, and V. Lupei, Appl. Phys. Lett. **82**, 844 (2003).

Optics Letters

Title Details

Related Titles

- **Alternative Media Edition** (4)

Lists

Marked Titles (0)

Search History

1539-4794 - (1)

Save to List Email Download Print Corrections Expand All Collapse All

Basic Description

Title	Optics Letters
ISSN	1539-4794
Publisher	Optical Society of America
Country	United States
Status	Active
Frequency	Semi-monthly
Language of Text	Text in: English
Refereed	Yes
Abstracted / Indexed	Yes
Serial Type	Journal
Content Type	Academic / Scholarly
Format	Online
Website	http://www.opticsinfobase.org
Description	Covers the latest research in optical science, including atmospheric optics, quantum electronics, fourier optics, integrated optics, and fiber optics.

- Subject Classifications
- Additional Title Details
- Publisher & Ordering Details
- Price Data
- Online Availability
- Abstracting & Indexing
- Other Availability
- Demographics

Save to List Email Download Print Corrections Expand All Collapse All